

Synergy between DUNE and T2HKK to probe Invisible Neutrino Decay

Zannatun Firdowzy Dey^{1,*} and Debajyoti Dutta^{1,2,†}

¹*Assam Don Bosco University, Tapesia Campus, Sonapur, Assam, 782402, India*

²*Bhattadev University, Pathsala Town, Barpeta, Assam 781325*

Abstract

We address the consequence of invisible neutrino decay within the framework of two long base-line neutrino experiments: T2HKK (Tokai-to-Hyper-Kamiokande-to-Korea) and DUNE (Deep Underground Neutrino experiment). Our primary objective is to bring out the aspects of CC (charged current) and NC (neutral current) measurements at DUNE in the context of invisible neutrino decay. We find that the inclusion of NC measurements with the CC measurements enhances its ability to constrain invisible neutrino decay. Further, the synergy between DUNE and T2HKK improves the constraints on invisible neutrino decay. At 3σ C.L. (confidence level) the derived constraint is $\tau_3/m_3 \geq 6.21 \times 10^{-11}$ s/eV. Additionally, if nature prefers ν_3 to be unstable and the decay width is $\tau_3/m_3 = 2.2 \times 10^{-11}$ s/eV, this combination can exclude the no-decay scenario at more than 5σ C.L. Although the CP sensitivity is not much hindered in the presence of invisible neutrino decay, the measurements of θ_{23} and the ability to resolve octant of θ_{23} is significantly influenced in these individual experiments. In the presence of invisible neutrino decay, the synergy between DUNE and T2HKK can exclude the wrong octant somewhat more effectively than either experiment alone.

* zannatundey@gmail.com

† debajyotidutta.hep@gmail.com

Contents

1 Introduction	2
2 Theory of invisible neutrino decay	6
3 Experimental and simulation details	7
3.1. DUNE	7
3.2. T2HKK	8
4 Results	9
4.1. Probability at DUNE and T2HKK	9
4.2. χ^2 analysis	11
1. Constraints on Invisible Neutrino Decay	11
2. Measurements of θ_{23} in the presence of Invisible Neutrino Decay	15
3. Octant of θ_{23} and CP violation Sensitivity in the presence of Invisible Neutrino Decay	15
4. Correlation plots	19
5 Summary and Conclusion	21

1. Introduction

The discovery of neutrino oscillations has led to a new area of research Beyond the Standard Model (BSM), explaining the existence of neutrino mass. Out of the six oscillation parameters, θ_{12}, θ_{13} and Δm_{21}^2 are measured precisely. However, the sign of Δm_{31}^2 , octant, absolute value of θ_{23} and the CP violating phase δ_{CP} are yet to be measured precisely. There are few indications regarding these unknown neutrino oscillation parameters from the ongoing neutrino oscillation experiments T2K [1] and NO ν A [2]. Both the experiments predict the same best-fit value for $\sin^2 \theta_{23}$ at 1σ C.L. Yet they have strong disagreements on the measured best-fit value of δ_{CP} . With more data from these experiments or from a combined analysis of the present data, better constraints can be put on these oscillation parameters. In these contexts, the upcoming experiments like DUNE[3–9], T2HK/T2HKK[10, 11],

ESS ν SB[12], JUNO[13], INO[14], PINGU[15], KM3Net-ORCA[16] etc. are aiming to determine these unknown parameters with more precision. In the present scenario, BSM physics such as the existence of sterile neutrinos, vector and scalar non-standard interactions (NSIs), invisible neutrino decay, etc., are some interesting topics to be explored further, as the presence of such new physics will affect the measurements of the standard neutrino oscillation parameters in these upcoming experiments. These long and short-baseline neutrino experiments will be able to address some of the questions.

Invisible neutrino decay is a new topic of interest, which was first proposed by ref. [17] to explain the solar neutrino problem. There are two possible modes of neutrino decay: visible and invisible decay. Both Dirac and Majorana neutrinos can undergo invisible decay. For Dirac neutrinos, the coupling between the neutrinos and the light scalar boson (s) leads to the decay mode: $\nu_j \rightarrow \bar{\nu}_{iR} + \chi$, where $\bar{\nu}_{iR}$ is the right-handed singlet and χ is the iso-singlet scalar. If neutrinos are Majorana particles, then the decay mode is $\nu_j \rightarrow \nu_s + J$, where ν_s is the sterile neutrino and J is a Majoron coupled by a pseudo-scalar coupling. This Majoron has to be singlet as constrained by the LEP data [18]. In both scenarios, the decay products are sterile and are invisible to the detectors. If the neutrino decays via $\nu_j \rightarrow \nu_i + J$ and $\nu_j \rightarrow \bar{\nu}_i + J$ channels, then the final states can be detected, and these modes of decay are known as visible neutrino decay. In visible neutrino decay, the final state fermion is a lighter neutrino, which is visible to the detectors, while in the other case, the final state particle, being a sterile neutrino, cannot be detected.

Assuming ν_2 to be unstable, neutrino decay with oscillation has been studied in [19–22]. These studies put constraints on the lifetime of ν_2 . In [23] solar neutrino data provide a constraint at $\tau_2/m_2 > 8.5 \times 10^{-7}$ s/eV. Constraints on both τ_2 and τ_1 have also been derived from low-energy solar neutrino data and supernova neutrino observations [24]. The lifetime of ν_e is strongly constrained by SN1987A data [25]. Earlier, to overcome the atmospheric neutrino problem, the possibility of neutrino decay was proposed in [26] but the fit was very poor. In [27, 28], authors studied neutrino decay with mixing to fit Super-Kamiokande (SK) data. Later, in [29] the SK collaboration showed that its data could better fit neutrino oscillation only. However, scenarios where an unstable neutrino decays to a sterile neutrino with $\Delta m^2 \sim 0.003$ eV² show potential for improving the fit to SK data [30]. So decay with oscillation can still give a better fit to SK data. Global analyses combining MINOS and atmospheric data have placed constraints such as $\tau_3/m_3 \geq 2.9 \times 10^{-10}$ s/eV at 90% C.L

[31]. Bounds on τ_3/m_3 considering two generations of neutrinos have been calculated using MINOS and T2K data in [32]. Using the preliminary data, the T2K and NO ν A experiments provide further insights, indicating $\tau_3/m_3 > 1.5 \times 10^{-12}$ s/eV at 3σ C.L. [33]. In [34], authors have presented constraints using data from NO ν A, T2K, MINOS/MINOS+, and their combinations assuming NO(IO) and at 90% C.L. the bounds are $3.0(2.9) \times 10^{-12}$ s/eV, $9.9(7.0) \times 10^{-12}$ s/eV, $1.6(1.8) \times 10^{-11}$ s/eV and $2.4(2.4) \times 10^{-11}$ s/eV respectively. Authors in [35] have also explored the implications of invisible neutrino decay, such as its potential to resolve discrepancies between track and cascade observations at IceCUBE. Authors of [36] have done an interesting analysis of the oscillation probabilities in the presence of invisible neutrino decay using the well-known Cayley-Hamilton formalism.

Numerous studies in the literature have explored the prospective capabilities of forthcoming experiments in detecting invisible decay. In the context of invisible neutrino decay, the performance of DUNE has been studied in [37]. A runtime of 5+5 years at DUNE is expected to yield constraints of $\tau_3/m_3 > 4.50 \times 10^{-11}$ s/eV at 90% C.L. Incorporating NC measurements with CC measurements at DUNE is anticipated to further enhance this constraint [38]. Additionally, the MOMENT experiment is projected to achieve bounds of $\tau_3/m_3 > 1.6 \times 10^{-11}$ s/eV at 3σ C.L. [39]. The ESS ν SB experiment, as discussed in [40], demonstrates significant potential with 3σ bounds on τ_3 at different baselines. Specifically, at 540 km, the constraints are less stringent compared to the 360 km baseline. Furthermore, the combined sensitivity of T2HK+ESS ν SB is expected to constrain $\tau_3/m_3 \geq 4.36 \times 10^{-11}$ s/eV at 3σ C.L., while T2HKK+ESS ν SB could achieve $\tau_3/m_3 \geq 5.53 \times 10^{-11}$ s/eV at the same confidence level [41] and at 3σ C.L. The JUNO experiment, detailed in [42], expects to set a stringent constraint of $\tau_3/m_3 > 7.5 \times 10^{-11}$ s/eV at 95% C.L. with 100 kt.years exposure. With a total exposure of 70 ton.year, solar data using high-resolution multi-ton Xenon detectors can constrain τ_2/m_2 and τ_1/m_1 at 2σ C.L. and the bounds are $\tau_2/m_2 > 8 \times 10^{-3}$ s/eV and $\tau_1/m_1 > 3 \times 10^{-2}$ s/eV, respectively [43]. If $\alpha_i = m_i/\tau_i$ is the decay parameter (where index i indicates mass eigenstate) then 10 years of solar data may provide stringent bounds on α_1 and α_2 and at 2σ C.L., the bounds are $\alpha_1 < 7.8 \times 10^{-15}$ eV² and $\alpha_2 < 2.3 \times 10^{-14}$ eV² respectively [44]. Visible neutrino decay is also tightly constrained, with analyses conducted in the context of long-baseline experiments [45–47].

Neutrino physics is in its precision era and upcoming neutrino experiments strive to achieve precise measurements of neutrino oscillation parameters. However, the existence

of parameter degeneracy [48] among the mixing parameters introduces challenges in accurately determining these parameters. Amalgamating different neutrino experiments helps in resolving parameter degeneracy. In this paper, we perform a synergistic study of DUNE and T2HKK in the context of invisible neutrino decay. Both DUNE and T2HKK are two promising upcoming long-baseline neutrino experiments. DUNE is a beam-based high-statistics experiment with a large detector mass, long baseline, and sufficient matter effect. On the other hand, T2HKK is also a very special experiment where it has two detector sites, and the detectors are placed close to their 1st and 2nd oscillation maxima. It also has a huge detector mass, huge statistics, and sufficient sensitivity to the matter effect, like DUNE. So combining such long-baseline experiments enhances overall sensitivity and aids in identifying potential synergies among the experiments.

Although separate studies have been performed in the presence of invisible neutrino decay at DUNE and T2HKK, we perform a combined study of these two experiments to explore possible synergies among them. Regarding DUNE, we individually investigate the sensitivity to τ_3/m_3 for both CC and NC measurements, and then combine the NC with CC. With the combined CC and NC measurements at DUNE, we incorporate data from the T2HKK experiment to get further enhanced limits on τ_3/m_3 . Even while NC events can be measured in water quite effectively, the migration matrix that reconstructs the neutrino events in T2HKK is not available to us. We have not performed NC analysis for T2HKK since it is inappropriate to use a Gaussian energy resolution function in this situation. The analysis is performed within the framework of three-flavour neutrino oscillation scenarios in the presence of matter effect. Additionally, we extensively study the correlations between θ_{23} and τ_3/m_3 . We thoroughly investigate how the presence of invisible neutrino decay, if it occurs naturally, affects the octant of θ_{23} and the CP violation sensitivities at the far detectors of DUNE and T2HKK. The same is also explored for the combination of the two experiments.

This paper is structured as follows: We address the theory of invisible neutrino decay in Section 2. In Section 3 we give a brief description of the two experiments and the simulation details. Our results are presented in Section 4 and we conclude in Section 5.

2. Theory of invisible neutrino decay

We suppose that the heaviest mass eigenstate ν_3 is not stable and undergoes decay into a sterile state, ν_4 , with lifetime τ_3 into a new sterile state and a scalar singlet J ; ($\nu_3 \rightarrow \bar{\nu}_4 + J$). Additionally, we assume that there is no mixing of the three active neutrinos with the sterile neutrino. Taking this into account, the neutrino mixing matrix can be described using the standard three-family mixing matrix U in the following manner

$$\begin{pmatrix} \nu_\alpha \\ \nu_s \end{pmatrix} = \begin{pmatrix} U & 0 \\ 0 & 1 \end{pmatrix} \begin{pmatrix} \nu_i \\ \nu_4 \end{pmatrix} \quad (1)$$

Where U is the standard PMNS (Pontecorvo–Maki–Nakagawa–Sakata matrix) matrix describing the standard three neutrino oscillation, $\alpha \rightarrow \nu_e, \nu_\mu, \nu_\tau$ indicates the flavour eigenstate and $i = 1, 2, 3$ the mass eigenstates. We assume normal mass ordering ($m_3 > m_1$) throughout this work. Furthermore, we assume that the mass and decay eigenstates are identical. Based on these presumptions, the evolution of neutrinos in the presence of matter can be expressed as follows:

$$i \frac{d}{dx} \begin{pmatrix} \nu_e \\ \nu_\mu \\ \nu_\tau \end{pmatrix} = \left[U \left[\frac{1}{2E} \begin{pmatrix} 0 & 0 & 0 \\ 0 & \Delta m_{21}^2 & 0 \\ 0 & 0 & \Delta m_{31}^2 \end{pmatrix} - i \frac{m_3}{2E\tau_3} \begin{pmatrix} 0 & 0 & 0 \\ 0 & 0 & 0 \\ 0 & 0 & 1 \end{pmatrix} \right] U^\dagger + \begin{pmatrix} A_{cc} & 0 & 0 \\ 0 & 0 & 0 \\ 0 & 0 & 0 \end{pmatrix} \right] \begin{pmatrix} \nu_e \\ \nu_\mu \\ \nu_\tau \end{pmatrix} \quad (2)$$

Simplifying the equation 2 we can write,

$$i \frac{d}{dx} v_f = \frac{1}{2E} [U \widetilde{H} U^\dagger + A] v_f. \quad (3)$$

Where,

$$\widetilde{H} = \begin{pmatrix} 0 & 0 & 0 \\ 0 & \Delta m_{21}^2 & 0 \\ 0 & 0 & \Delta m_{31}^2 - \frac{im_3}{\tau_3} \end{pmatrix}, A = \begin{pmatrix} A_{cc} & 0 & 0 \\ 0 & 0 & 0 \\ 0 & 0 & 0 \end{pmatrix} \quad (4)$$

Here $A_{cc} = 2\sqrt{2}G_F n_e E$ represents the matter potential due to neutrino electron scattering, G_F is the Fermi coupling constant, E is the energy and n_e is the density of the

electron. The probability of getting a neutrino from an initial state ν_a to a final state ν_b can be expressed as

$$P_{ab} = | \langle \nu_b | \nu_a \rangle |^2. \quad (5)$$

Where, a , and b correspond the flavour states e , μ , and τ . The decay rate of the unstable state ν_3 is defined as m_3/τ_3 . Therefore, in the probability equation, the effect of the decay appears as $\exp [-(m_3/\tau_3)\frac{L}{E}]$. Hence, a lower value of the decay parameter will affect an experiment with a longer baseline or lower energy.

3. Experimental and simulation details

DUNE and T2HKK are two long baseline experiments. In this section, we give a brief description of these two experiments.

3.1. DUNE

DUNE (Deep Underground Neutrino Experiment)[3–9] plans to shoot a special beam of neutrinos (and their anti-particles) from Fermilab in Illinois. A 120 GeV proton beam with a beam power of 1.2 MW, will hit the graphite target each year to produce around 1.1×10^{21} protons. As a result, charged mesons will be produced, which will decay in flight into neutrinos. The underground far detector will be installed in South Dakota, 1285 km away from the source at Fermilab. The net volume of the Liquid Argon (LAr) detector at the far site will be 40 kt, and in this analysis, we assume a single-phase detector [4]. The whole experiment is set to run for 10 years, spending equal time on neutrinos and anti-neutrinos. The key scientific objectives of the DUNE experiment involve measuring the CP phase, determining neutrino mass ordering, identifying the mixing angle θ_{23} and its octant, and examining the three-neutrino paradigm. A significant focus is on the search for CP violation in neutrino oscillations, which could provide insights into the matter-antimatter asymmetry. DUNE also endeavours to explore the phenomenon of proton decay. The experiment seeks to enhance its capability to detect neutrinos emitted from core-collapse supernovae and to explore phenomena beyond the scope of the SM [4].

Our results are obtained using the DUNE simulation configuration given in ref. [49]. For the analysis of CC, we have used the 0.125 GeV energy binning approach with reconstructed

energies E_{rec} spanning from 0 to 110 GeV. This range is divided into 64 bins spanning from 0 to 8 GeV, each bin being 0.125 GeV wide. The remaining 16 bins cover the range from 8 to 110 GeV, with varying widths. For the analysis of NC, we have used the migration matrices from ref. [50] and the bin size of the used migration matrices is 50 MeV. Therefore in this work, we have also used energy bins of 50 MeV for NC events. We assumed a detection efficiency of 90% for NC events.

3.2. T2HKK

The next Hyper-K experiment is planned to construct two identical water-Cherenkov detectors, each 187 kt in size. The first will be located at the Tochibora mine in Japan, with a baseline of 295 km from the J-PARC neutrino target and an off-axis angle of 2.5° . The other detector may be located in Korea at a baseline of 1100 km. The flux at 295 km will cover the first oscillation maximum and the flux at 1100 km will cover the second oscillation maximum. The first and second oscillation maxima of the PMNS neutrino appearance probability can be reached due to Korea's longer baseline. The longer baseline of the Korean sites improves the oscillation probability's CP-violating component and resolves parameter combinations between the CP-violating phase and neutrino mass ordering that would be almost degenerate if measurements were limited to the Japanese site. T2HKK offers a baseline that is nearly as long as the proposed DUNE experiment, but it is in an energy band that is similar to that of the current T2K experiment. This enables it to probe oscillations at the second oscillation maximum, a capability that is only shared by the proposed ESS neutrino beam and not available to any other experiment[51].

In our analysis, we have used GLoBES (General Long Baseline Neutrino Experiment simulator) [52] software package to simulate the DUNE and T2HKK experiments. We have simulated DUNE for a run time of 10 years, which is equally divided between neutrinos and anti-neutrinos. Similarly, for T2HKK we have considered a run time of 2.5 years for neutrinos and 7.5 years for anti-neutrinos, respectively. For the energy resolution of T2HKK, we have assumed a Gaussian function of width $15\%/\sqrt{E}$. Table I provides the values of the three neutrino oscillation parameters that we used in our simulation. The values provided in the table align with the current global fit ranges [53]. The calculations have been done considering normal mass ordering. The signal and background normalization uncertainties

Parameter	Best-fit Value	3σ range
θ_{13}	8.6°	$[8.1^\circ, 8.9^\circ]$
θ_{12}	33.82°	$[31.3^\circ, 35.9^\circ]$
θ_{23}	41.95° (LO), 48.44° (HO)	$[38^\circ, 52^\circ]$
Δm_{21}^2 (eV 2)	7.39×10^{-5}	$[6.82, 8.04] \times 10^{-5}$
Δm_{31}^2 (eV 2)	2.52×10^{-3}	$[2.43, 2.60] \times 10^{-3}$
δ_{CP}	-90°	$[-180^\circ, 180^\circ]$

Table I. The best-fit values of the neutrino oscillation parameters and the corresponding 3σ allowed ranges.

Experiment	Signal						Background				
	App. ν	App. $\bar{\nu}$	Disapp. ν	Disapp. $\bar{\nu}$	NC	tilt	$\nu_e, \bar{\nu}_e$ CC	$\nu_\mu, \bar{\nu}_\mu$ CC	$\nu_\tau, \bar{\nu}_\tau$ CC	NC	tilt
DUNE	2%	2%	5%	5%	5%	5%	5%	5%	20%	10%	10%
T2HKK	3.2%	3.9%	3.6%	3.6%	-	5%	5%	5%	-	-	10%

Table II. signal and background uncertainties associated with DUNE and T2HKK.

of DUNE and T2HKK experiments for various channels used in this analysis are given in Table II.

4. Results

In this section, we present the results of our analysis.

4.1. Probability at DUNE and T2HKK

In Figure 1, we present the probability of neutrino oscillations for the DUNE and T2HKK experiments as a function of energy. The figure illustrates probabilities for both appearance (left) and disappearance (right) channels, comparing scenarios with and without invisible

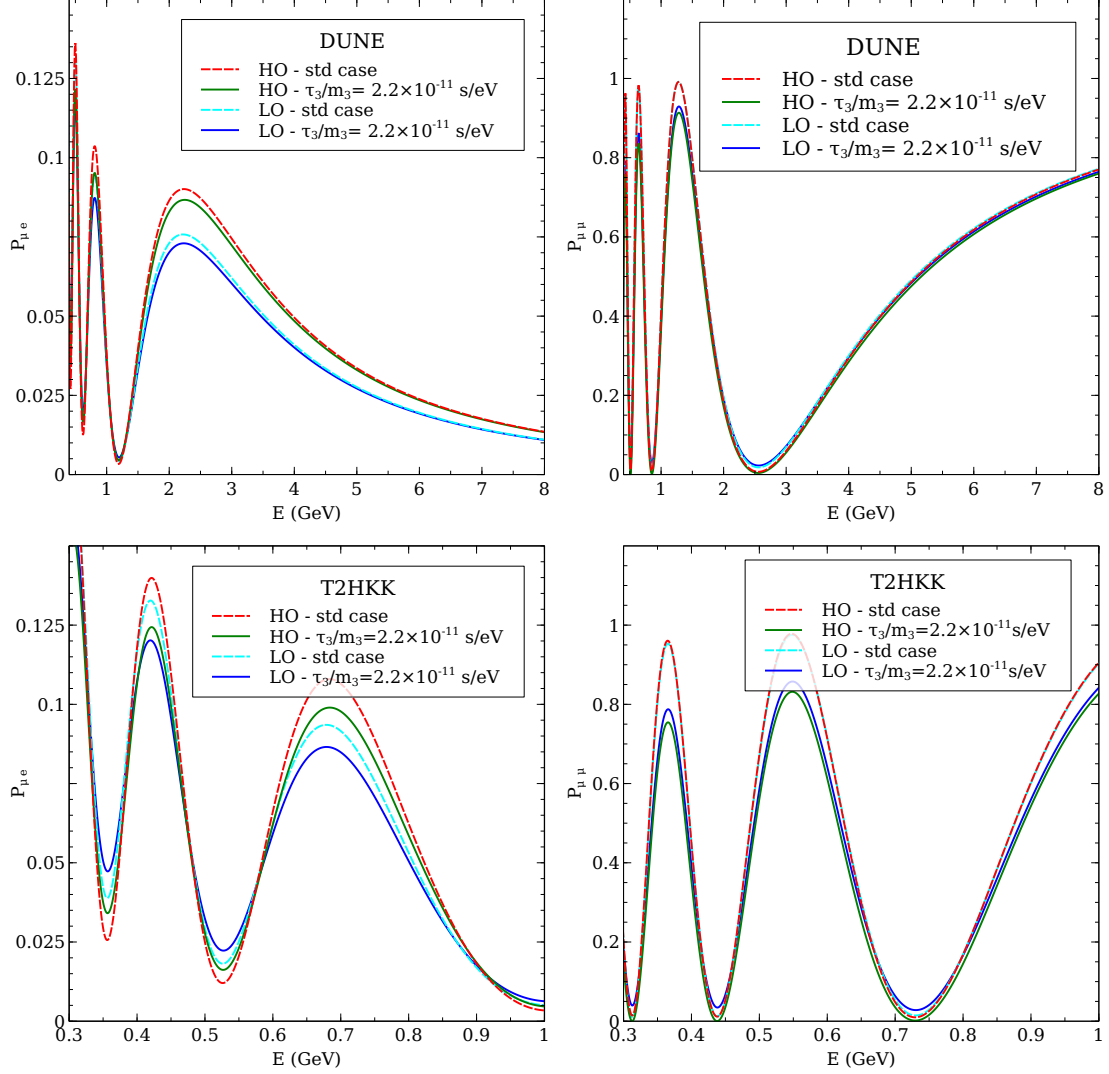


Figure 1. The appearance (left panels) and disappearance (right panels) channels of neutrino oscillation probabilities for DUNE and T2HKK experiments as a function of neutrino energy. The top panel corresponds to DUNE, and the bottom panel corresponds to T2HKK.

neutrino decay. In the top panel, we present the probability plots for the DUNE and the bottom panel shows the probability plots for T2HKK. For all the cases, the dashed lines are for standard oscillation case and the solid lines are for $\tau_3/m_3 = 2.2 \times 10^{-11}$ s/eV. We show the results for both the lower octant ($\theta_{23} = 41.95^\circ$) and the higher octant ($\theta_{23} = 48.44^\circ$). The red (cyan) dashed lines represent the probability of no decay in HO (LO), while the green (blue) solid lines represent probability plots in the presence of invisible neutrino decay in HO (LO).

From Figure 1, we observe that $P_{\mu e}$ decreases in the presence of neutrino decay both

in the lower and the higher octants. For a fixed value of $\tau_3/m_3 = 2.2 \times 10^{-11}$ s/eV the probability in the lower octant is smaller than the probability in the higher octant. Also around the oscillation maxima, the effect of decay is more prominent in T2HKK than DUNE. The disappearance probabilities ($\nu_\mu \rightarrow \nu_\mu$) are shown in the right panel of Figure 1. The disappearance probability plots for the no decay case overlap in both the lower and the higher octants and this behavior is the same in both DUNE and T2HKK. But in the presence of neutrino decay, the disappearance probability decreases. Around the oscillation peaks, the difference is significant, especially in T2HKK. This is clear from the following two-generation survival probability in a vacuum [41]:

$$P_{\mu\mu} = [1 - \sin^2 \theta_{23}(1 - e^{-\frac{m_3 L}{\tau_3 E}})]^2 - \sin^2 2\theta_{23} e^{-\frac{m_3 L}{\tau_3 2E}} \sin^2\left(\frac{\Delta m_{31}^2 L}{4E}\right) \quad (6)$$

In the case when there is no decay, the probability is determined by $\sin^2 2\theta_{23}$. However, when decay is present, the $e^{-\frac{m_3 L}{\tau_3 E}}$ factor becomes significant and causes octant sensitivity.

4.2. χ^2 analysis

1. Constraints on Invisible Neutrino Decay

In this section, we perform a χ^2 analysis to show how these experiments and their combinations can constrain invisible neutrino decay. We have estimated the statistical χ^2 function using the following relation:

$$\chi_{stat}^2 = 2 \sum_i \left[N_i^{test} - N_i^{true} + N_i^{true} \log \frac{N_i^{true}}{N_i^{test}} \right] \quad (7)$$

Where N_i^{true} represents the number of true events and N_i^{test} represents the number of test events. True events are generated for the given true values in Table I and the χ^2 is computed for a given set of true values by marginalizing over the test parameters in their 3σ allowed ranges. The uncertainties mentioned in Table II are incorporated in the χ^2 by ‘‘pull’’ method using the following expression:

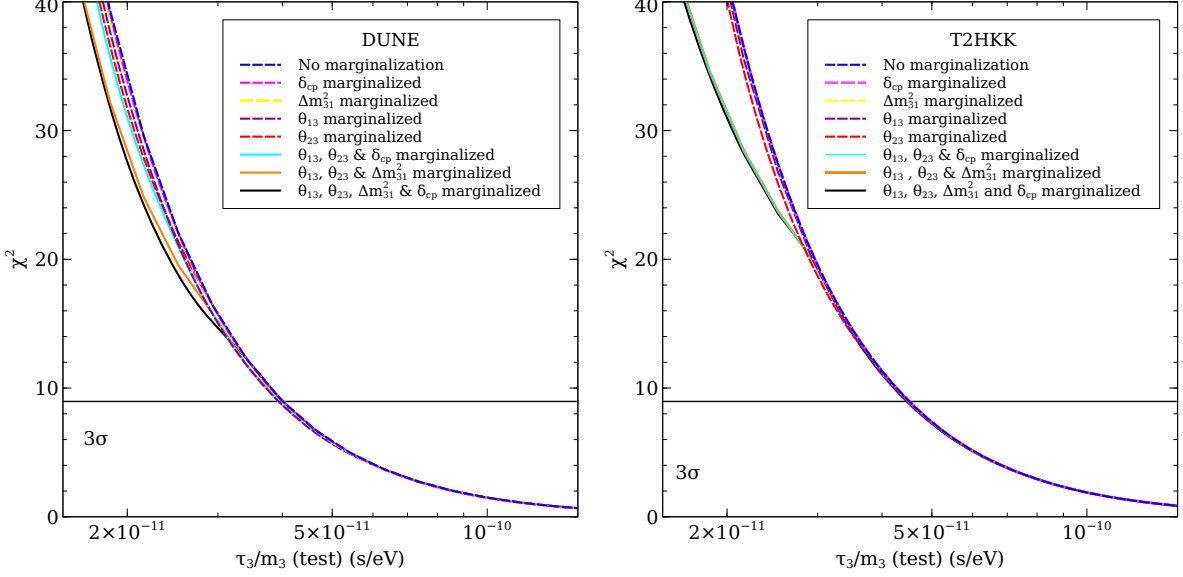


Figure 2. The sensitivity χ^2 as a function of τ_3/m_3 for DUNE and T2HKK for different marginalization effects. The left panel is for DUNE and the right panel is for T2HKK. The data have been generated for the no-decay scenario.

$$N_i^{\text{test}} = \sum_{s(b)} N_i^{s(b)} \left(1 + c_i^{s(b)\text{norm}} \xi^{s(b)\text{norm}} + c_i^{s(b)\text{tilt}} \xi^{s(b)\text{tilt}} \frac{E_i - \bar{E}}{E_{\text{max}} - E_{\text{min}}} \right) \quad (8)$$

Here in this equation, $s(b)$ denotes signal(background), $\xi^{\text{norm}}(\xi^{\text{tilt}})$ is the “pull” variable and $c_i^{\text{norm}}(c_i^{\text{tilt}})$ represents the change in the number of events due to the variation of the “pull” variable. In the above equation, E_i is the mean reconstructed energy of the i^{th} bin and the mean energy is given by, $\bar{E} = (E_{\text{max}} + E_{\text{min}})/2$ (E_{min} and E_{max} respectively are the maximum and minimum energy of the energy range).

Here we present the χ^2 sensitivity as a function of the decay parameter. We explore the effect of different marginalization while constraining invisible neutrino decay. The results are shown in Figure 2. The data in all the cases shown in Figure 2 are generated with the standard oscillation parameters given in Table I. The true value of θ_{23} is considered in the higher octant, i.e., $\theta_{23} = 48.44^\circ$. The blue dashed lines represent the scenario where we have not marginalized any parameters. The dashed magenta, yellow, purple, and red lines represent the marginalization of δ_{CP} , Δm_{31}^2 , θ_{13} , and θ_{23} respectively in their 3σ allowed range. The solid cyan and brown lines represent the cases where the marginalization is done over θ_{13} , θ_{23} , δ_{CP} and θ_{13} , θ_{23} , Δm_{31}^2 respectively. Finally, the black lines show the effect of

marginalization over θ_{13} , θ_{23} , Δm_{31}^2 and δ_{CP} .

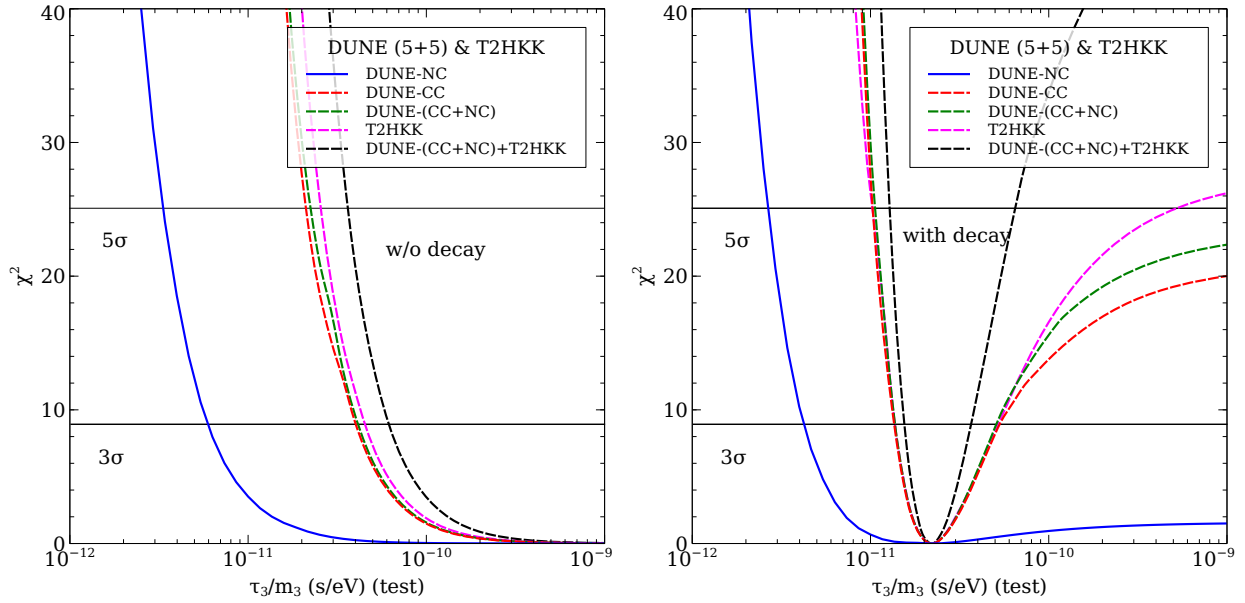


Figure 3. χ^2 as a function of τ_3/m_3 for standalone and combination of experiments. The left panel is for no-decay in data and the right panel is for $\tau_3/m_3 = 2.2 \times 10^{-11}$ s/eV in data.

In Figure 2, we observe that at DUNE, the dashed blue line aligns closely with both the dashed magenta and yellow lines, indicating that marginalization over Δm_{31}^2 and δ_{CP} has minimal impact on constraining invisible neutrino decay. The effects primarily arise from variations in θ_{13} and θ_{23} . Again, marginalizing over θ_{13} , θ_{23} , and Δm_{31}^2 (represented by the brown line) significantly influences the constraint, with further adjustments possible upon inclusion of δ_{CP} . Similarly, for T2HKK, marginalizing over Δm_{31}^2 and δ_{CP} shows negligible effects, while marginalization over θ_{13} influences the constraint. However, marginalization over θ_{23} shows observable effects. Notably, when considering constraints obtained by marginalizing over different combinations of parameters, such as θ_{13} , θ_{23} , Δm_{31}^2 (represented by the brown lines), θ_{13} , θ_{23} , and δ_{CP} (represented by the cyan lines), and θ_{13} , θ_{23} , Δm_{31}^2 , and δ_{CP} (represented by the black lines), they all exhibit almost identical behaviour. Hence, unless otherwise specified, we adopt marginalization over θ_{13} , θ_{23} , Δm_{31}^2 , and δ_{CP} for both experiments throughout the remainder of this study.

In Figure 3, we show the sensitivities of DUNE, T2HKK, and their combinations to invisible neutrino decay. The results are shown for DUNE-NC, DUNE-CC, DUNE-(CC+NC),

T2HKK, and DUNE-(CC+NC)+T2HKK. We consider the true value of θ_{23} in the higher octant (HO), which is 48.44° . The blue solid lines in Figure 3 represent DUNE-NC, the red dashed lines represent DUNE-CC, the magenta dashed lines represent T2HKK, the green dashed lines represent DUNE-(CC+NC), and the dashed black lines represent the combination of DUNE-(CC+NC) and T2HKK. In the left panel, the data is generated with the value of the oscillation parameters as given in Table I. These plots show how well DUNE, T2HKK, and their combinations can constrain invisible neutrino decay. In the left panel, we see that the inclusion of the neutral current with the charged current slightly improves the limits on the decay parameter. Additionally, the combination of DUNE-(CC+NC)+T2HKK provides the highest limit on the decay parameter. After 10 years (5 years of ν and 5 years of $\bar{\nu}$) of running of DUNE, the limits obtained by DUNE-CC, DUNE-(CC+NC), and DUNE-(CC+NC)+T2HKK are 4.07×10^{-11} s/eV, 4.22×10^{-11} s/eV and 6.21×10^{-11} s/eV, respectively, at a 3σ C.L. Notably, the constraint obtained from T2HKK is 4.39×10^{-11} s/eV at the same C.L. which is better than DUNE-(CC+NC).

The right panel of Figure 3 shows how these experiments and their combinations can exclude the present standard oscillation scenario if invisible neutrino decay is a natural phenomenon with $\tau_3/m_3 = 2.2 \times 10^{-11}$ s/eV. The true value of τ_3/m_3 considered in this work is within the allowed region of T2K, NO ν A and MINOS/MINOS+ data analysis [34]. So if ν_3 is unstable in nature with a decay width $\tau_3/m_3 = 2.2 \times 10^{-11}$ s/eV, then DUNE, after running for 10 years (5 years of ν and 5 years of $\bar{\nu}$), can exclude no-decay scenario at 3σ C.L., whereas T2HKK alone can exclude the same at more than 5σ C.L. The synergy between DUNE and T2HKK can further improve the exclusion limit to 5σ C.L. It can be seen from the Figure 3 that, T2HKK has better precision than DUNE. For a given true value of $\tau_3/m_3 = 2.2 \times 10^{-11}$ s/eV, T2HKK can measure the decay parameter within the range $[5.31 \times 10^{-11} > \tau_3/m_3 > 1.35 \times 10^{-11}]$ s/eV at 3σ C.L. On the other hand, DUNE-(CC+NC) can precisely measure the decay parameter within the range $[5.16 \times 10^{-11} > \tau_3/m_3 > 1.35 \times 10^{-11}]$ s/eV at 3σ C.L. for the same value of decay parameter. The synergy between DUNE and T2HKK improves the precision further and can measure the decay parameter within the range $[6.44 \times 10^{-11} > \tau_3/m_3 > 1.28 \times 10^{-11}]$ s/eV ($[3.64 \times 10^{-11} > \tau_3/m_3 > 1.55 \times 10^{-11}]$ s/eV) at 5σ (3σ) C.L.

2. Measurements of θ_{23} in the presence of Invisible Neutrino Decay

In this section, we show the effect of invisible neutrino decay in the measurements of θ_{23} . We show the results considering $\theta_{23} = 48.44^\circ$ at the higher octant. In the standard case, the true value of the decay parameter is zero while in the presence of invisible neutrino decay, the considered true value of the decay parameter is $\tau_3/m_3 = 2.2 \times 10^{-11}$ s/eV. Figure 4 shows the results of this analysis. The dashed red line represents the standard scenario while the dashed black line represents the decay scenario (non-zero decay in data). In the fit we have marginalized over θ_{13} , Δm_{31}^2 and δ_{CP} in their 3σ allowed range.

From this analysis, we have observed that the position of the global minima changes in both the octants if invisible neutrino decay is a natural phenomenon. In the case of DUNE, (Figure 4), the global true minima for the stable neutrino scenario is situated at the higher octant (HO) at $\theta_{23} = 48.44^\circ$ (as expected) while the fake minima appear in the LO at $\theta_{23} = 44.07^\circ$. However, the inclusion of neutrino decay alters the positions of these minima in both the octants. At DUNE, the χ^2 minima shifts to $\theta_{23} = 47.72^\circ$ in the HO, while in the LO, fake minima appears at $\theta_{23} = 44.16^\circ$. This behaviour is consistent in both DUNE and T2HKK, as well as in their combined analyses. In T2HKK, in the presence of neutrino decay, the minima in the HO occur at $\theta_{23} = 47.89^\circ$, and fake minima appear in LO at $\theta_{23} = 43.62^\circ$. For the combination of DUNE and T2HKK, the minima in the HO shifts to $\theta_{23} = 47.86^\circ$ and in the LO, it appears at $\theta_{23} = 43.79^\circ$. This shift in the positions of χ^2 minima is comprehensively discussed in [37, 41].

3. Octant of θ_{23} and CP violation Sensitivity in the presence of Invisible Neutrino Decay

In this section, we study the effect of invisible neutrino decay in the measurements of octant and CP violation sensitivity at the far detector of these experiments. Figure 5 and 6 show the octant resolution capacity and the CP violation sensitivity for DUNE-(CC+NC), T2HKK, and the combination of DUNE-(CC+NC) and T2HKK respectively. To address the ability of the considered experiments to rule out the wrong octant, we vary the true θ_{23} in the range $[38^\circ, 52^\circ]$, keeping the true values of all other oscillation parameters fixed at their best-fit values(as given in I). In the presence of invisible neutrino decay, a non-zero

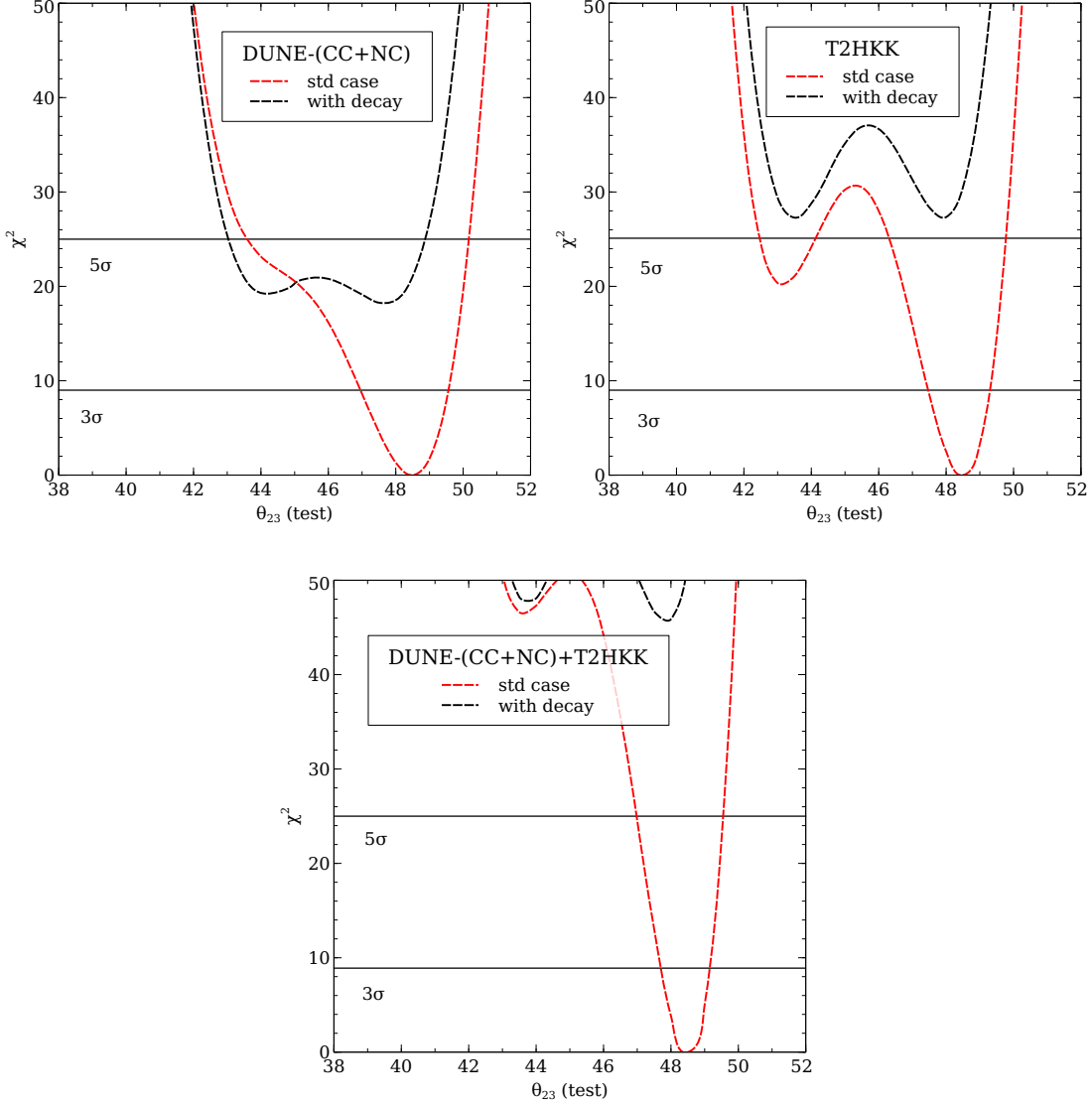


Figure 4. χ^2 as a function of $\sin^2\theta_{23}$ (test). The top left panel corresponds to DUNE-(CC+NC), the top right panel corresponds to the combination of both experiments. The dashed red line is for the stable neutrino case while the dashed black line represents the decay scenario.

value of the decay parameter ($\tau_3/m_3 = 2.2 \times 10^{-11}$ s/eV) is considered in the data. We show the χ^2 as a function of true θ_{23} assuming NH as the true hierarchy. In the fit we marginalize over θ_{13} , Δm_{31}^2 and δ_{CP} in their allowed 3σ range. Also, for every true value of θ_{23} in the lower octant (LO), we vary the test θ_{23} in the higher octant (HO) and vice-versa. In Figure 5, the dashed red line represents the standard oscillation scenario while the dashed black line represents the decay scenario. If neutrino decay is a natural occurrence, it will change the capabilities of these experiments to resolve octant degeneracy. In standard oscillation

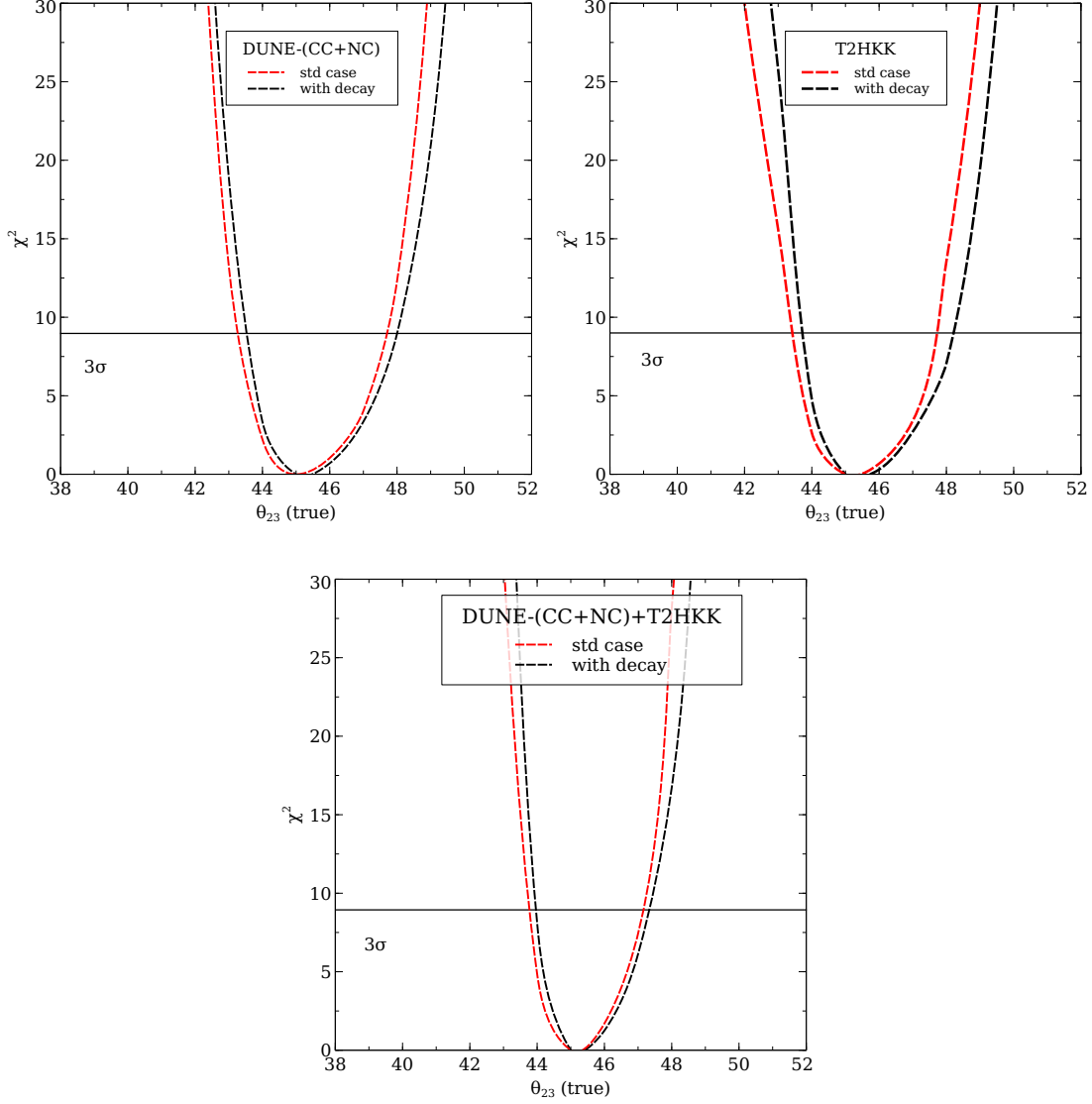


Figure 5. Expected octant-sensitivity at DUNE-(CC+NC) top left, T2HKK top right , and DUNE-(CC+NC)+T2HKK bottom panel. The red dashed lines are for standard oscillation case and the black dashed lines are in the presence of invisible neutrino decay.

case, DUNE (T2HKK) can fix octant degeneracy for all true $\theta_{23} \leq 43.28^\circ$ ($\theta_{23} \leq 43.39^\circ$) and $\theta_{23} \geq 47.72^\circ$ ($\theta_{23} \geq 47.75^\circ$) at 3σ . In this case, the combination of DUNE(CC+NC) and T2HKK can rule out the wrong octant at 3σ for all true $\theta_{23} \leq 43.76^\circ$ and $\theta_{23} \geq 47.18^\circ$. At DUNE (T2HKK), in the presence of neutrino decay, octant resolution is possible for all true $\theta_{23} \leq 43.53^\circ$ ($\theta_{23} \leq 43.73^\circ$) and $\theta_{23} \geq 48^\circ$ ($\theta_{23} \geq 48.23^\circ$) at 3σ . The combination can resolve octant at 3σ for all true $\theta_{23} \leq 43.99^\circ$ and $\theta_{23} \geq 47.38^\circ$ respectively. Therefore, in comparison to the standard oscillation scenario, the octant resolving capabilities of these

setups slightly improve in the LO but deteriorate in the HO in the presence of invisible neutrino decay. Based on the foregoing analysis, we find that in the presence of invisible neutrino decay, the combined effect of DUNE and T2HKK can exclude the wrong octant somewhat more effectively than either experiment alone.

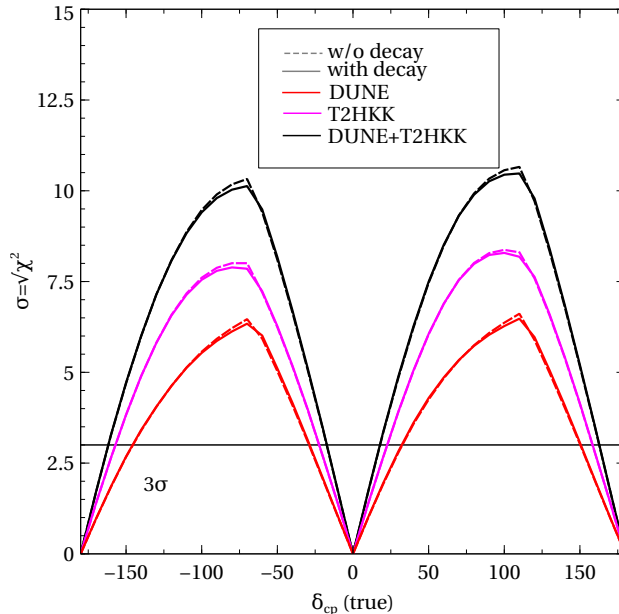


Figure 6. CP violation sensitivity for DUNE-(CC+NC) (red), T2HKK (magenta), and DUNE-(CC+NC)+T2HKK (black) experiments. The dashed lines are for the standard oscillation case and the solid lines are for the decay case.

In Figure 6, we present the CP violation sensitivity plots for DUNE-(CC+NC), T2HKK, and the combination of DUNE-(CC+NC) and T2HKK. The true value of θ_{23} considered in this case is 48.44° . Here, all the solid lines represent the decay scenario, while the dashed lines represent the stable neutrino case. In Figure 6 the red lines depict DUNE-(CC+NC), magenta lines represent T2HKK, and the black lines represent DUNE-(CC+NC)+T2HKK. CP violation sensitivity of an experiment is the measure of its ability to exclude the CP-conserving values. To measure the CP violation sensitivity, we vary the true δ_{CP} within the range $[-\pi, \pi]$ in data while in the fit, we fix δ_{CP} at 0 and $\pm\pi$. The oscillation parameters θ_{13} , θ_{23} and Δm_{31}^2 are marginalized in their 3σ range keeping the other parameter fixed as given in Table I. We see that the invisible neutrino decay brings no noticeable change in the CP sensitivity plots.

4. Correlation plots

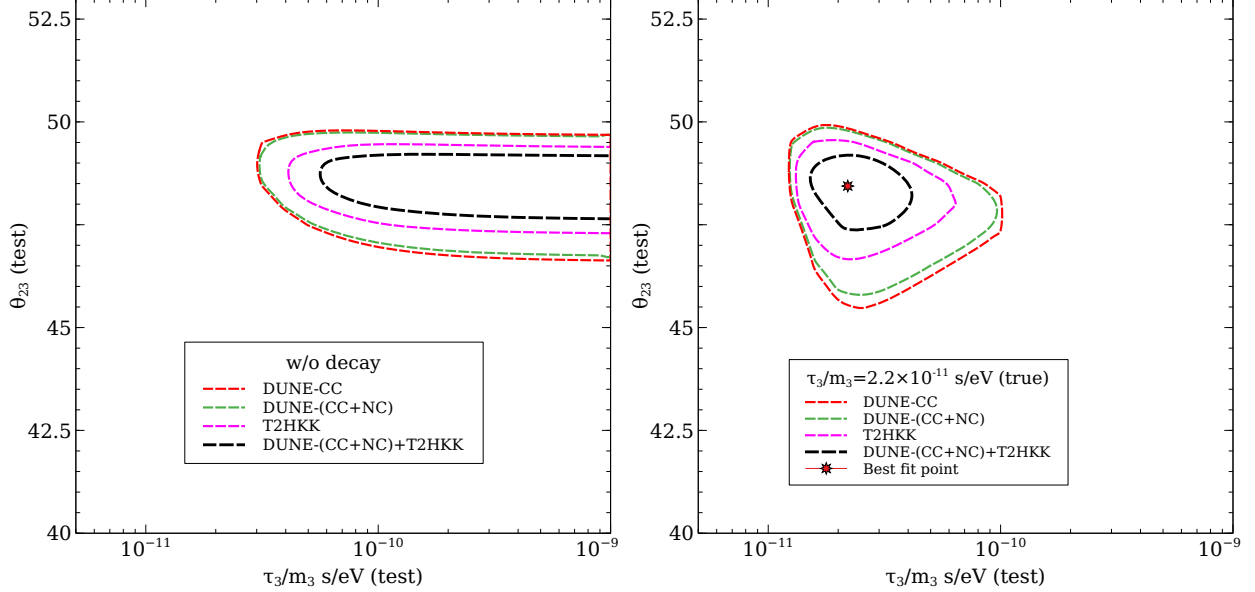


Figure 7. The 3σ confidence contours in the $\tau_3/m_3 - \theta_{23}$ plane for DUNE (CC-red lines, CC+NC-green lines), T2HKK (magenta lines) and DUNE-(CC+NC)+T2HKK (black lines). The left panel is for no-decay scenario and the right panel is for $\tau_3/m_3 = 2.2 \times 10^{-11}$ s/eV in data.

In Figure 7, we present the correlation between τ_3/m_3 and θ_{23} at 3σ C.L. in $\tau_3/m_3 - \theta_{23}$ plane. The results are generated for DUNE, T2HKK and for their combinations. In the left panel, we consider the no-decay scenario and in the right panel, we assume that neutrino decay is a natural phenomenon in addition to oscillations. In the analysis, we use the true value of the atmospheric mixing angle $\theta_{23} = 48.44^\circ$ and the true value of the decay parameter $\tau_3/m_3 = 2.2 \times 10^{-11}$ s/eV. This plot complements the results shown in Figure 3 but in $\tau_3/m_3 - \theta_{23}$ plane. The smaller the parameter space, the more precise the measurements are. For DUNE, parameter space shrinks slightly in both panels when we add neutral current measurements to the charged current measurements. However, T2HKK performs better than DUNE in both scenarios. If neutrino decays in addition to oscillation, then T2HKK can significantly constrain the parameter space and hence can make more precise measurements in the 3σ allowed region. The combinations of DUNE and T2HKK enhance the precision. In this case, the synergy between DUNE and T2HKK aids in all aspects to

probe invisible neutrino decay.

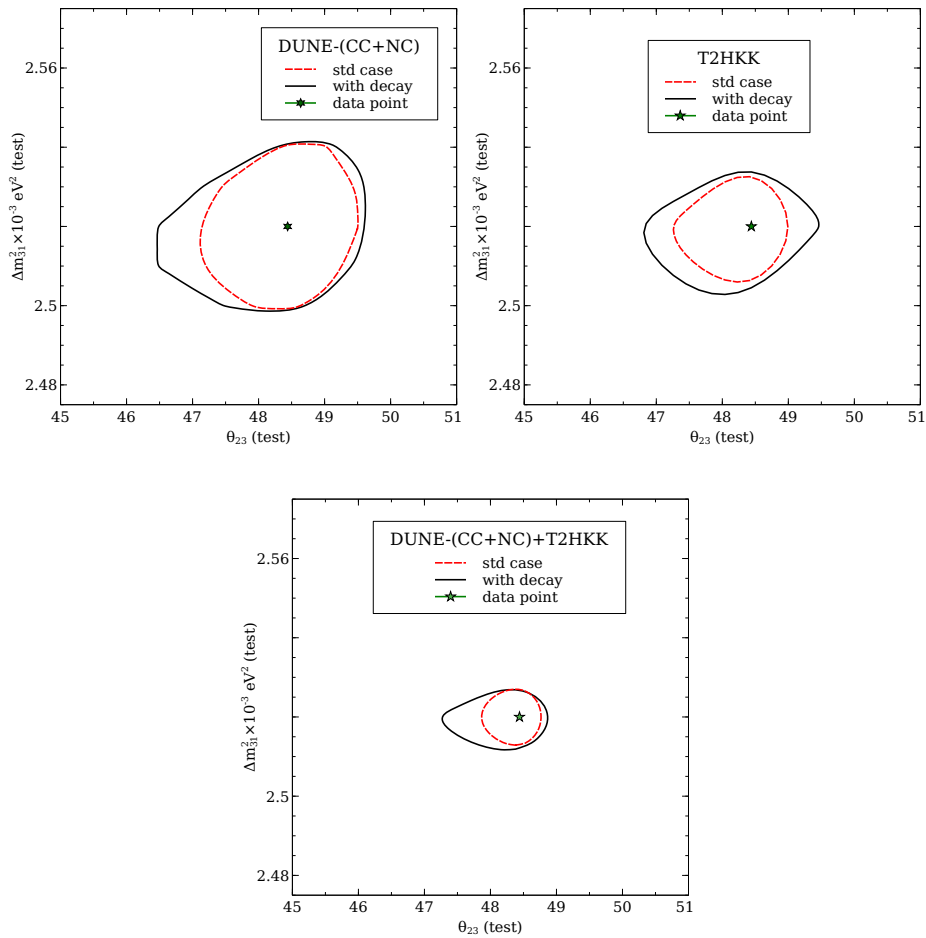


Figure 8. The 3σ confidence contours in the $\theta_{23} - \Delta m_{31}^2$ plane for DUNE-(CC+NC) (top left), T2HKK (top right), and DUNE-(CC+NC)+T2HKK (bottom) experiments. The red dashed contours are for standard oscillation case and solid black contours are for $\tau_3/m_3 = 2.2 \times 10^{-11}$ s/eV.

In Figure 2, we have already observed the effects of θ_{23} and Δm_{31}^2 on constraining invisible neutrino decay. Both parameters play an important role in the presence of invisible neutrino decay. Here in Figure 8, we show the 3σ allowed region in $\theta_{23} - \Delta m_{31}^2$ plane for DUNE, T2HKK and for the combination of both the experiments, with and without neutrino decay. For all the cases in Figure 8 the red dashed contours represent the stable neutrino case while the solid black contours represent the decay case. For the standard oscillation case, the contours are marginalized over θ_{13} and δ_{CP} in their current 3σ ranges. While for the decay case, we have varied the decay parameter in the range 10^{-12} to 10^{-9} (s/eV) along

with the marginalization of θ_{13} and δ_{CP} in their current 3σ ranges. We observe that in the presence of invisible neutrino decay with oscillation, the allowed region increases more than the standard case, in all three cases. The precision of measurement at T2HKK is higher than that of DUNE as the $\theta_{23} - \Delta m_{31}^2$ parameter space shrinks in the case of T2HKK. The precision of measurements increases when we combine both experiments. In table III, we present a comparison of the limit on decay parameters obtained from various experiments.

5. Summary and Conclusion

Invisible neutrino decay could have a major role in cosmology. Assuming that the neutrinos are stable, the bound on the sum of neutrino masses is measured in the cosmological timescale which are much stronger than the bounds from oscillation experiments. If invisible neutrino decay is a natural phenomenon, it may alter the equation of the state of the Universe and, consequently, the CMB spectra. As a result, the bound on the sum of neutrino masses may become less stringent [55, 56], but the allowed values of τ/m are much larger. Hence, if one observed an anomalous signal in oscillation experiments, it would have an important impact on Cosmology.

In this work, we have explored the impact of invisible neutrino decay in two upcoming long baseline experiments, DUNE and T2HKK. We assumed that the mass eigenstate m_3 is heavier than m_4 and hence ν_3 being unstable can decay to a lighter sterile state. Throughout this analysis, we have assumed normal mass hierarchy as the true hierarchy. Here, we have combined the neutral current measurements and charged current measurements at DUNE to constrain invisible neutrino decay. We found that this combination of CC and NC enhances DUNE's ability to constrain τ_3/m_3 . We found that the synergy between DUNE and T2HKK can provide tight constraints on τ_3/m_3 .

Firstly, we have checked the effect of marginalization on constraining invisible neutrino decay. It is observed that the marginalization of Δm_{31}^2 and δ_{CP} have a minimal effect while that of θ_{13} and θ_{23} have a significant effect on invisible neutrino decay, especially at DUNE. Based on this analysis, we have considered the marginalization of θ_{13} , θ_{23} , Δm_{31}^2 and δ_{CP} while deriving the constraint on invisible neutrino decay. We found that after taking data for 10 years, DUNE (with both CC and NC measurements) at 3σ C.L. can constrain τ_3/m_3 at 4.22×10^{-11} s/eV. We have observed that the T2HKK experiment has a better ability to

Experiment	90% C.L. (3σ) bound on τ_3/m_3 (s/eV)	Ref.
SK+MINOS	$2.9(0.54) \times 10^{-10}$	Ref. [31]
T2K + NO ν A	$2.3(1.5) \times 10^{-12}$	Ref. [33]
T2K+NO ν A+MINOS	$2.4(2.4) \times 10^{-11}$	Ref. [34]
DUNE - CC	$4.50(2.38) \times 10^{-11}$	Ref. [37]
DUNE - (CC+NC) (5+5)	$5.1(2.7) \times 10^{-11}$	Ref. [38]
T2HKK	$8.41 \times 10^{-11}(4.39 \times 10^{-11})$	This work
DUNE - (CC+NC) (5+5)	$7.74(4.22) \times 10^{-11}$	This work
DUNE - (CC+NC) (5+5)+T2HKK	$1.12 \times 10^{-10}(6.21 \times 10^{-11})$	This work
ESSnuSB (540 km)	$4.22(1.68) \times 10^{-11}$	Ref. [40]
ESSnuB (360 km)	$4.95(2.64) \times 10^{-11}$	Ref. [40]
JUNO	$9.3(4.7) \times 10^{-11}$	Ref. [42]
INO	$1.51(0.566) \times 10^{-10}$	Ref. [54]
KM3NeT-ORCA	$2.5(1.4) \times 10^{-10}$	Ref. [16]
T2HK	$4.43(2.72) \times 10^{-11}$	Ref. [41]
T2HKK	$1.01 \times 10^{-10}(4.36 \times 10^{-11})$	Ref. [41]
T2HKK+ESSnuSB	$1.064 \times 10^{-10}(5.53 \times 10^{-11})$	Ref. [41]
ESSnuSB	$3.69(2.43) \times 10^{-11}$	Ref. [41]
T2HK+ESSnuSB	$1.01 \times 10^{-10}(4.36 \times 10^{-11})$	Ref. [41]

Table III. Comparison of bound on decay parameter τ_3/m_3 from various experiments. The bounds for SK+MINOS, T2K+NO ν A and T2K+NO ν A+MINOS are based on actual observational data.

constrain invisible neutrino decay than DUNE. This constraint on invisible decay improves further when combined with the DUNE experiment and at 3σ C.L., the bound obtained is 6.21×10^{-11} s/eV. If nature has invisible neutrino decay in addition to oscillations and the true value of $\tau_3/m_3 = 2.2 \times 10^{-11}$ s/eV, the synergy between these two experiments can rule out a stable neutrino scenario up to 5σ C.L. In that case, the combination of DUNE and T2HKK can measure the decay parameter within the range $[6.44 \times 10^{-11} > \tau_3/m_3 > 1.28 \times 10^{-11}]$ s/eV.

The impact of decay in θ_{23} measurement has also been studied. We have found that the θ_{23} measurements are hampered in the presence of invisible neutrino decay. If the data is generated with neutrino decay, both the true and fake minima deviate from the minima corresponding to the stable neutrino. If neutrino decay is a natural process, then the measurements of θ_{23} get affected which is also seen from the correlation plots in the $\tau_3/m_3 - \theta_{23}$ plane.

This study also reveals that in the presence of invisible neutrino decay, the ability of these experiments to rule out the wrong octant changes as compared to the stable neutrino scenario. The octant resolving capabilities of these setups slightly improve in the LO but deteriorate in the HO in the presence of invisible neutrino decay. The effect of invisible neutrino decay in the measurement of CP violation sensitivity is nominal.

While the NC measurements at DUNE have no significant effect on invisible neutrino decay, combining it with the CC measurements provides higher precision. Furthermore, combining DUNE-(CC+NC) with T2HKK improves the constraints on the decay parameter.

References

- [1] K. Abe *et al.* (T2K), *Phys. Rev. Lett.* **118**, 151801 (2017), [arXiv:1701.00432 \[hep-ex\]](#).
- [2] P. Adamson *et al.* (NOvA), *Phys. Rev. Lett.* **116**, 151806 (2016), [arXiv:1601.05022 \[hep-ex\]](#).
- [3] B. Abi *et al.* (DUNE), *JINST* **15**, T08008 (2020), [arXiv:2002.02967 \[physics.ins-det\]](#).
- [4] B. Abi *et al.* (DUNE), (2020), [arXiv:2002.03005 \[hep-ex\]](#).
- [5] B. Abi *et al.* (DUNE), *JINST* **15**, T08009 (2020), [arXiv:2002.03008 \[physics.ins-det\]](#).
- [6] B. Abi *et al.* (DUNE), *JINST* **15**, T08010 (2020), [arXiv:2002.03010 \[physics.ins-det\]](#).
- [7] B. Abi *et al.* (DUNE), *Eur. Phys. J. C* **81**, 322 (2021), [arXiv:2008.12769 \[hep-ex\]](#).
- [8] A. Abed Abud *et al.* (DUNE), (2022), [arXiv:2203.06100 \[hep-ex\]](#).
- [9] B. Abi *et al.* (DUNE), *Eur. Phys. J. C* **80**, 978 (2020), [arXiv:2006.16043 \[hep-ex\]](#).
- [10] K. Abe *et al.* (Hyper-Kamiokande Proto-), *PTEP* **2015**, 053C02 (2015), [arXiv:1502.05199 \[hep-ex\]](#).
- [11] H.-K. proto Collaboration, K. Abe, K. Abe, S. Ahn, H. Aihara, A. Aimi, R. Akutsu, C. Andreopoulos, I. Anghel, L. Anthony, *et al.*, *Progress of Theoretical and Experimental Physics* **2018**, 063C01 (2018).
- [12] E. Baussan *et al.* (ESSnuSB), *Nucl. Phys. B* **885**, 127 (2014), [arXiv:1309.7022 \[hep-ex\]](#).
- [13] F. An *et al.* (JUNO), *J. Phys. G* **43**, 030401 (2016), [arXiv:1507.05613 \[physics.ins-det\]](#).
- [14] S. Ahmed *et al.* (ICAL), *Pramana* **88**, 79 (2017), [arXiv:1505.07380 \[physics.ins-det\]](#).
- [15] M. G. Aartsen *et al.* (IceCube-PINGU), (2014), [arXiv:1401.2046 \[physics.ins-det\]](#).
- [16] P. F. de Salas, S. Pastor, C. A. Ternes, T. Thakore, and M. Tórtola, *Phys. Lett. B* **789**, 472 (2019), [arXiv:1810.10916 \[hep-ph\]](#).
- [17] J. N. Bahcall, N. Cabibbo, and A. Yahil, *Phys. Rev. Lett.* **28**, 316 (1972).
- [18] S. Pakvasa, *AIP Conf. Proc.* **542**, 99 (2000), [arXiv:hep-ph/0004077](#).
- [19] A. Acker and S. Pakvasa, *Phys. Lett. B* **320**, 320 (1994), [arXiv:hep-ph/9310207](#).
- [20] S. Choubey, S. Goswami, and D. Majumdar, *Phys. Lett. B* **484**, 73 (2000), [arXiv:hep-ph/0004193](#).
- [21] A. Bandyopadhyay, S. Choubey, and S. Goswami, *Phys. Rev. D* **63**, 113019 (2001), [arXiv:hep-ph/0101273](#).
- [22] A. S. Joshipura, E. Masso, and S. Mohanty, *Phys. Rev. D* **66**, 113008 (2002), [arXiv:hep-ph/0203181](#).
- [23] A. Bandyopadhyay, S. Choubey, and S. Goswami, *Phys. Lett. B* **555**, 33 (2003), [arXiv:hep-](#)

ph/0204173.

- [24] J. M. Berryman, A. de Gouvea, and D. Hernandez, *Phys. Rev. D* **92**, 073003 (2015), [arXiv:1411.0308 \[hep-ph\]](#).
- [25] J. A. Frieman, H. E. Haber, and K. Freese, *Phys. Lett. B* **200**, 115 (1988).
- [26] J. M. LoSecco, (1998), [arXiv:hep-ph/9809499](#).
- [27] V. D. Barger, J. G. Learned, S. Pakvasa, and T. J. Weiler, *Phys. Rev. Lett.* **82**, 2640 (1999), [arXiv:astro-ph/9810121](#).
- [28] P. Lipari and M. Lusignoli, *Phys. Rev. D* **60**, 013003 (1999), [arXiv:hep-ph/9901350](#).
- [29] Y. Ashie *et al.* (Super-Kamiokande), *Phys. Rev. Lett.* **93**, 101801 (2004), [arXiv:hep-ex/0404034](#).
- [30] S. Choubey and S. Goswami, *Astropart. Phys.* **14**, 67 (2000), [arXiv:hep-ph/9904257](#).
- [31] M. C. Gonzalez-Garcia and M. Maltoni, *Phys. Lett. B* **663**, 405 (2008), [arXiv:0802.3699 \[hep-ph\]](#).
- [32] R. A. Gomes, A. L. G. Gomes, and O. L. G. Peres, *Phys. Lett. B* **740**, 345 (2015), [arXiv:1407.5640 \[hep-ph\]](#).
- [33] S. Choubey, D. Dutta, and D. Pramanik, *JHEP* **08**, 141 (2018), [arXiv:1805.01848 \[hep-ph\]](#).
- [34] C. A. Ternes and G. Pagliaroli, (2024), [arXiv:2401.14316 \[hep-ph\]](#).
- [35] P. B. Denton and I. Tamborra, *Phys. Rev. Lett.* **121**, 121802 (2018), [arXiv:1805.05950 \[hep-ph\]](#).
- [36] J. Grönroos, T. Ohlsson, and S. Vihonen, (2024), [arXiv:2401.16864 \[hep-ph\]](#).
- [37] S. Choubey, S. Goswami, and D. Pramanik, *JHEP* **02**, 055 (2018), [arXiv:1705.05820 \[hep-ph\]](#).
- [38] A. Ghoshal, A. Giarnetti, and D. Meloni, *J. Phys. G* **48**, 055004 (2021), [arXiv:2003.09012 \[hep-ph\]](#).
- [39] J. Tang, T.-C. Wang, and Y. Zhang, *JHEP* **04**, 004 (2019), [arXiv:1811.05623 \[hep-ph\]](#).
- [40] S. Choubey, M. Ghosh, D. Kempe, and T. Ohlsson, *JHEP* **05**, 133 (2021), [arXiv:2010.16334 \[hep-ph\]](#).
- [41] K. Chakraborty, D. Dutta, S. Goswami, and D. Pramanik, *JHEP* **08**, 136 (2021), [arXiv:2012.04958 \[hep-ph\]](#).
- [42] T. Abrahão, H. Minakata, H. Nunokawa, and A. A. Quiroga, *JHEP* **11**, 001 (2015), [arXiv:1506.02314 \[hep-ph\]](#).
- [43] G.-Y. Huang and S. Zhou, *JCAP* **02**, 024 (2019), [arXiv:1810.03877 \[hep-ph\]](#).

- [44] P. Martínez-Miravé, I. Tamborra, and M. Tórtola, (2024), [arXiv:2402.00116 \[astro-ph.HE\]](#).
- [45] A. M. Gago, R. A. Gomes, A. L. G. Gomes, J. Jones-Perez, and O. L. G. Peres, *JHEP* **11**, 022 (2017), [arXiv:1705.03074 \[hep-ph\]](#).
- [46] P. Coloma and O. L. G. Peres, (2017), [arXiv:1705.03599 \[hep-ph\]](#).
- [47] M. V. Ascencio-Sosa, A. M. Calatayud-Cadenillas, A. M. Gago, and J. Jones-Pérez, *Eur. Phys. J. C* **78**, 809 (2018), [arXiv:1805.03279 \[hep-ph\]](#).
- [48] V. Barger, D. Marfatia, and K. Whisnant, *Phys. Rev. D* **65**, 073023 (2002), [arXiv:hep-ph/0112119](#).
- [49] B. Abi *et al.* (DUNE), (2021), [arXiv:2103.04797 \[hep-ex\]](#).
- [50] V. De Romeri, E. Fernandez-Martinez, and M. Sorel, *JHEP* **09**, 030 (2016), [arXiv:1607.00293 \[hep-ph\]](#).
- [51] K. Abe *et al.* (Hyper-Kamiokande), *PTEP* **2018**, 063C01 (2018), [arXiv:1611.06118 \[hep-ex\]](#).
- [52] P. Huber, M. Lindner, and W. Winter, *Comput. Phys. Commun.* **167**, 195 (2005), [arXiv:hep-ph/0407333](#).
- [53] I. Esteban, M. C. Gonzalez-Garcia, M. Maltoni, T. Schwetz, and A. Zhou, *JHEP* **09**, 178 (2020), [arXiv:2007.14792 \[hep-ph\]](#).
- [54] S. Choubey, S. Goswami, C. Gupta, S. M. Lakshmi, and T. Thakore, *Phys. Rev. D* **97**, 033005 (2018), [arXiv:1709.10376 \[hep-ph\]](#).
- [55] Z. Chacko, A. Dev, P. Du, V. Poulin, and Y. Tsai, *JHEP* **04**, 020 (2020), [arXiv:1909.05275 \[hep-ph\]](#).
- [56] M. Escudero, J. Lopez-Pavon, N. Rius, and S. Sandner, *JHEP* **12**, 119 (2020), [arXiv:2007.04994 \[hep-ph\]](#).